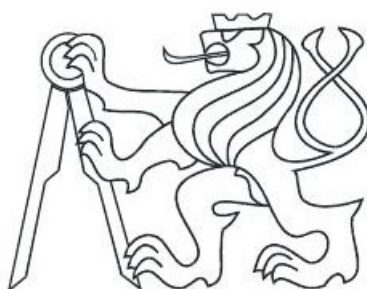


Czech Technical University in Prague  
Faculty of Nuclear Sciences and Physical Engineering



**Study of jet production in the d+Au and Au+Au  
collisions at RHIC**

**Research Work**

*Author:* Jan Rusňák

*Supervisor:* RNDr. Jana Bielčíková, PhD.

Prague, 2009

*název práce:* **Studium jetů v d+Au a Au+Au srážkách na urychlovači RHIC**

*autor:* Jan Rusňák

*obor:* Jaderné inženýrství

*druh práce:* Výzkumný úkol

*vedoucí práce:* RNDr. Jana Bielčíková, Ph.D.

*konzultant:* Mgr. Jan Kapitán

*abstrakt:* Experiment STAR na urychlovači RHIC se zabývá studiem jaderné hmoty v extrémních podmínkách vysokých teplot a hustot energie, která vzniká v jádro-jaderných srážkách při energii  $\sqrt{s_{NN}} = 200$  GeV. Jednou z nejdůležitějších sond této jaderné hmoty je studium produkce jetů a určení jejich modifikace při průchodu jadernou hmotou. Toto studium umožní získat detailnější znalosti o vlastnostech jaderné hmoty v extrémních podmínkách v porovnání s měřením inkluzivní produkce částic a dvou-částicových korelací.

*klíčová slova:* jety, STAR, jT, algoritmy na rekonstrukci jetů

*title:* **Study of jet production in the d+Au and Au+Au collisions at RHIC**

*author:* Jan Rusňák

*supervisor:* RNDr. Jana Bielčíková, Ph.D.

*consultant:* Mgr. Jan Kapitán

*abstract:* The STAR experiment at RHIC studies the extreme states of matter which forms in the nucleus-nucleus collisions at energies  $\sqrt{s_{NN}} = 200$  GeV. Jet production and the modification of their shape when passing through the hot bulk matter represent one of the most important probes of this matter. These measurements can give us more detailed information about the bulk matter than the measurements of inclusive particle production spectra and two-particle correlations.

*key words:* jets, STAR, jT, jet reconstruction algorithms

## **Prohlášení**

Prohlašuji, že jsem tento výzkumný úkol vypracoval samostatně a použil jsem pouze podklady (literaturu, projekty, SW atd.) uvedené v příloženém seznamu. Nemám závažný důvod proti použití tohoto školního díla ve smyslu § 60 Zákona č.121/2000 Sb., o právu autorském, o právech souvisejících s právem autorským a o změně některých zákonů (autorský zákon).

V Praze dne 16.9.2009

Jan Rusňák

# Contents

|  |           |
|--|-----------|
| <b>Preface</b>                                     | <b>5</b>  |
| <b>1 Introduction</b>                              | <b>6</b>  |
| 1.1 Jets   | 6         |
| 1.2 Jets and QCD                                   | 7         |
| <b>2 Jet Reconstruction Algorithms</b>             | <b>10</b> |
| 2.1 Requirements                                   | 10        |
| 2.2 Cone algorithms                                | 12        |
| 2.2.1 Midpoint algorithm                           | 12        |
| 2.2.2 SISCone algorithm                            | 13        |
| 2.3 Clustering algorithms                          | 14        |
| 2.3.1 $k_{\perp}$ algorithm                        | 14        |
| 2.3.2 Anti- $k_{\perp}$ algorithm                  | 14        |
| 2.3.3 $k_{\perp}$ vs. anti- $k_{\perp}$            | 14        |
| 2.3.4 Resolution parameter R                       | 15        |
| 2.4 FastJet  | 15        |
| 2.4.1 Speed  | 15        |
| 2.4.2 Jet areas                                    | 16        |
| <b>3 STAR Experiment</b>                           | <b>19</b> |
| 3.1 RHIC   | 19        |
| 3.2 STAR   | 20        |
| 3.2.1 Time Projection Chamber                      | 21        |
| 3.2.2 Electromagnetic Calorimeter                  | 22        |
| 3.2.3 Upgrades                                     | 22        |
| <b>4 Measurement of Jet <math>j_{\perp}</math></b> | <b>24</b> |
| 4.1 Jet $j_{\perp}$                                | 24        |
| 4.2 Analysis                                       | 25        |
| Summary and Outlook                                | 31        |
| <b>Bibliography</b>                                | <b>32</b> |

## Preface

Recent data obtained from the Relativistic Heavy Ion Collider show a significant suppression of high- $p_{\perp}$  particles in the central Au+Au collisions at  $\sqrt{s} = 200$  GeV in comparison with the p+p and d+Au data. This suppression is apparent from both hadron spectra and di-hadron correlations, which have represented until recently the main tools for studying the properties of the hot, strongly interacting matter formed at the central Au+Au collisions at RHIC [1, 2]. However, in a few recent years a big progress has been made on the field of the jet reconstruction [3]. Now it is possible to reconstruct the jets even in the Au+Au collisions at  $\sqrt{s} = 200$  GeV, despite of the enormous background. This give us an additional tool for studying the bulk matter. In order to separate the cold matter effects and the initial state effects from the final state effects it is necessary to perform additional experiments with lighter nuclei, concretely p+p and d+Au collisions. Jets reconstruction and study of some of their properties in the d+Au collisions is the main goal of this work.

# Chapter 1

## Introduction

### 1.1 Jets

In particle physics, jets are narrow sprays of particles, mainly hadrons. They are produced during high-energy collisions from partons (quarks and gluons) as a result of fragmentation and hadronization process. In high-energy p+p or ion collisions incident particles may get close enough that their partons scatter. The scattered partons cannot remain free and they soon hadronize, creating a shower of particles (mainly hadrons). Their momentum is collimated in a narrow cone. The higher is the parton's momentum the narrower is the cone. Such a cone of particles is what we usually call a jet.

The reason why we are so concerned in the observation of jets is that they possess the same kinematical properties as the original partons (total momentum, total energy). Thus the jets are a good probe of the QCD matter and a window to the world of the short-distance ( $\sim 1\text{fm}$ ) physics. What more, jets can be treated as infrared-safe objects, therefore there can be made calculations using the perturbative QCD (pQCD) in order to make theoretical predictions about jets.

In p-p collisions, the most common jet event is di-jet - the result of scattering of two partons from each one of the colliding protons.

Let's assume a (central) collision of two protons. In the center of mass system (CMS) their total momentum is zero. Two of their quarks can scatter to approximately<sup>1)</sup> opposite directions in the transversal plane ( $\Delta\phi \simeq \pi$ ). However, their momentum in the longitudinal direction (=beam direction) is  $x_1 P_1$  and  $x_2 P_2$ , where  $P_1, P_2$  are momenta of the colliding hadrons and  $x_1, x_2$  are Bjorken's scale variables of scattered partons. Since  $x_i \in (0, 1)$  and  $P_i$  values are large (hundreds of GeV), the size of the partons' longitudinal momentum can vary one from other a lot. Therefore the jets are not back-to-back in the beam direction. The (approximate) transversal back-to-back direction can be further affected by additional soft re-scattering (especially in the heavy ion collisions). Finally the quarks hadronize

---

<sup>1)</sup>In the protons' CMS the partons are not at rest - they can have relatively small (but non-negligible) momentum in the transversal direction therefore they don't fly away in the exactly opposite directions and with the exactly same energy - this is the cause of the jets' "intrinsic  $k_\perp$ ".

which results to formation of two jets. But if one of the quarks radiates a gluon before it hadronizes, the gluon can also fragment into a jet. That means we can also observe 3-jet, 4-jet, ... events. By studying the properties of di-jets one can obtain useful information about the medium surrounding the collision area.

It is anticipated that a dense, strongly interacting medium with deconfined and chiral symmetric quarks is formed in heavy ion collisions at energy densities above  $1 \text{ GeV}/\text{fm}^3$ . This new kind of matter - Quark Gluon Plasma (QGP) - would affect the passing quarks by the strong interaction.

Now imagine two scattered quarks surrounded by such matter. They are making their way through the medium and are losing their energy. Suddenly one of them gets out since the other is still on its draining way. They hadronize, but one of them has significantly lower energy. Since most of the energy of the parton is transmitted to only one (“leading”) hadron, the leading hadron of the second jet will have noticeable lower  $p_{\perp}$ . Second jet is “quenched”. The quenched jet will embody the following properties [6]: softer hadron spectra, larger multiplicity, increased angular broadening. Also the high- $p_{\perp}$  hadrons spectra will be suppressed, since the leading hadron of a quenched jet has significantly lower  $p_{\perp}$ . Jet quenching is a phenomena which has been observed in  $\sqrt{s_{\text{NN}}} = 200 \text{ GeV}$  Au+Au collisions at RHIC [13]. Whether it is a clear proof of the QGP is still a subject to discuss.

## 1.2 Jets and QCD

Quantum chromodynamics (QCD) is a non-Abelian gauge field theory of the strong interaction between quarks and gluons. There are two major properties of quarks and gluons described by the QCD.

- **Confinement:**

Quarks are fermions with electric charge  $-1/3e$  or  $2/3e$ . They also carry a color charge. Three types of color charge exist - “red”, “green”, “blue”. According to the QCD quarks cannot be separated singularly, they form only colorless objects - baryons (3 quarks:  $RGB$ ) and mesons (quark-antiquark:  $R\bar{R}, G\bar{G}, B\bar{B}$ ). If one tries to separate two quarks, the force between them rises and at some distance it is sufficient for creating a quark-antiquark pair which confines with the two “separated” quarks.

Gluons are vector gauge bosons that moderate the strong interaction. They also carry a color charge which means they can also interact between each other.

- **Asymptotic freedom:**

The strong coupling constant  $\alpha_S$  is not a true constant, but it “runs” with the space distance (or equivalently with high momentum transfers). In other words,  $\alpha_S(r)$  with the distance  $r \rightarrow 0$  (or  $q^2 \rightarrow \infty$ , where  $q^2$  is the momentum transfer e.g. between two colliding quarks) vanishes. Therefore the quarks inside a hadron feel (almost) no color force and behave as free particles. Moreover, at the distances  $\sim 1 \text{ fm}$  (or at sufficiently high momentum transfers) the coupling constant is small enough that the

QCD can be approached perturbatively. Perturbative QCD (pQCD) is a powerful tool for making theoretical predictions at the parton level.

## Parton distribution functions

When calculating the parton-parton scattering cross section, one has to take into account that partons (confined in a hadron) are not at rest, but carry a fraction of hadron's momentum. Therefore it is convenient to introduce the parton distribution function (PDF)  $f_i(x, Q^2)$  which express the probability of finding a parton  $i$  inside hadron carrying the hadron's momentum fraction  $x$ .  $Q^2$  is the momentum transfer between the scattering partons. The total cross section for a general hard process  $i+j \rightarrow k+X$  then can be calculated as

$$\sigma_{tot} = \sum_{i,j} \int_0^1 dx_1 \int_0^1 dx_2 \int d\hat{t} f_i(x_1, Q^2) f_j(x_2, Q^2) \frac{d\sigma_{ij \rightarrow kX}}{d\hat{t}}, \quad (1.1)$$

where  $\hat{t}$  is the Mandelstam variable and  $\frac{d\sigma_{ij \rightarrow kX}}{d\hat{t}}$  are differential cross sections of all possible processes  $i+j \rightarrow k+X$  ( $ud \rightarrow ud$ ,  $u\bar{u} \rightarrow d\bar{d}$ ,  $uu \rightarrow uu$ ,  $u\bar{u} \rightarrow d\bar{d}g$ , etc.). The  $Q^2$  dependence of the PDFs is described by DGLAP equations

$$\begin{aligned} Q^2 \frac{d}{d \log Q^2} f_g(x, Q^2) &= \frac{\alpha_s(Q^2)}{\pi} \int_x^1 \frac{dz}{z} P_{g \leftarrow q}(z) \sum_f \left[ f_f\left(\frac{x}{z}, Q^2\right) + f_{\bar{f}}\left(\frac{x}{z}, Q^2\right) \right] + \\ &\quad + P_{g \leftarrow g}(z) f_g\left(\frac{x}{z}, Q^2\right), \\ Q^2 \frac{d}{d \log Q^2} f_f(x, Q^2) &= \frac{\alpha_s(Q^2)}{\pi} \int_x^1 \frac{dz}{z} \left\{ P_{q \leftarrow q}(z) f_f\left(\frac{x}{z}, Q^2\right) + P_{q \leftarrow g}(z) f_g\left(\frac{x}{z}, Q^2\right) \right\}, \\ Q^2 \frac{d}{d \log Q^2} f_{\bar{f}}(x, Q^2) &= \frac{\alpha_s(Q^2)}{\pi} \int_x^1 \frac{dz}{z} \left\{ P_{q \leftarrow q}(z) f_{\bar{f}}\left(\frac{x}{z}, Q^2\right) + P_{q \leftarrow g}(z) f_g\left(\frac{x}{z}, Q^2\right) \right\}, \end{aligned} \quad (1.2)$$

where  $P_{i \leftarrow j}(z)$  are splitting functions describing the probability of finding the parton  $i$  inside the parton  $j$  carrying momentum fraction  $z$ .

However it is not possible to calculate the PDFs themselves by using the pQCD techniques. The lattice QCD calculations are extremely computationally demanding in this case and can be performed only in a few special cases. Therefore one have to determine the right form of the PDFs by fitting the experimental data, mainly from the deep inelastic scattering (DIS) experiments. It shows up that the PDFs of each particular type of hadron (e.g. proton) are universal in electro-weak interactions (it doesn't matter which probe we use for the DIS).

## Fragmentation

The scattered parton carries out a large amount of energy which it loses by gluon radiation and by the production of  $q\bar{q}$  pairs. The color charged partons cannot remain free and combine together, forming colorless hadrons. These processes are called fragmentation and

hadronization. Probability of finding a hadron  $h$  “inside” the original parton  $i$  carrying the momentum fraction  $x$  is given by fragmentation functions (FF)  $D_i^h(x, Q^2)$ . These have to be also obtained by fitting the data, e.g. from  $e^-e^+ \rightarrow q\bar{q}$  experiments. Also the FFs exhibit an universality, regardless of the origin of the quarks ( $p+p$  collision,  $e^-+p$  collision,  $e^-+e^+$  annihilation...).

## Divergences in pQCD

Now take a look at the cross section of the following simple process

$$e^- + e^+ \rightarrow q + \bar{q} + g$$

For the cross section holds the following proportionality

$$\frac{d\sigma}{dx_1 dx_2} \propto \frac{x_1^2 + x_2^2}{(1-x_1)(1-x_2)}, \quad x_i \equiv \frac{E_i}{\sqrt{\hat{s}}}, \quad (1.3)$$

where  $\hat{s}$  is the Mandelstam variable,  $E_1, E_2, E_3$  are energies of outgoing quark, antiquark and gluon respectively. It holds

$$x_1 = 1 - \frac{(p_2 + p_3)^2}{s}, \quad x_2 = 1 - \frac{(p_1 + p_3)^2}{s}. \quad (1.4)$$

Now we will investigate the divergencies in the equation (1.3). The limiting case  $x_1 \rightarrow 1$  represents the situation when the emitted gluon is collinear with the outgoing antiquark, while that with  $x_2 \rightarrow 1$  corresponds to the case when the gluon is collinear with the quark (“collinear” divergences). In third case  $x_1 = x_2 = 0$  the energy of the gluon vanishes (“infrared” divergence). To avoid these divergences higher orders of the perturbation theory have to be calculated in. What is important, not only the process  $e^-e^+ \rightarrow q\bar{q}g$  is affected by these divergences. They are a general property of the QCD.

# Chapter 2

## Jet Reconstruction Algorithms

### 2.1 Requirements

Unfortunately, it is a formidable task to clearly distinguish which particles belong to the jet, especially in the heavy ion collisions. One needs a reliable algorithm in order to fully reconstruct a jet from the collected data. A good algorithm should fulfill the following conditions:

- Order independence
- Infrared and collinear safe
- Easy to use
- Detector independent
- Highly effective
- With short computing time

**Order independence** - the algorithm should produce the same results at the parton level (when applied on theoretical calculations), hadron level (when applied on MC simulations) and at the detector level (when applied on experimental data), as illustrated on [Figure 2.1](#).

**Infrared safe** - the algorithm should be insensitive to any soft radiation in the event. This means that any radiated soft gluons (and products of their hadronization) will not affect the shape or even the number of reconstructed jets.

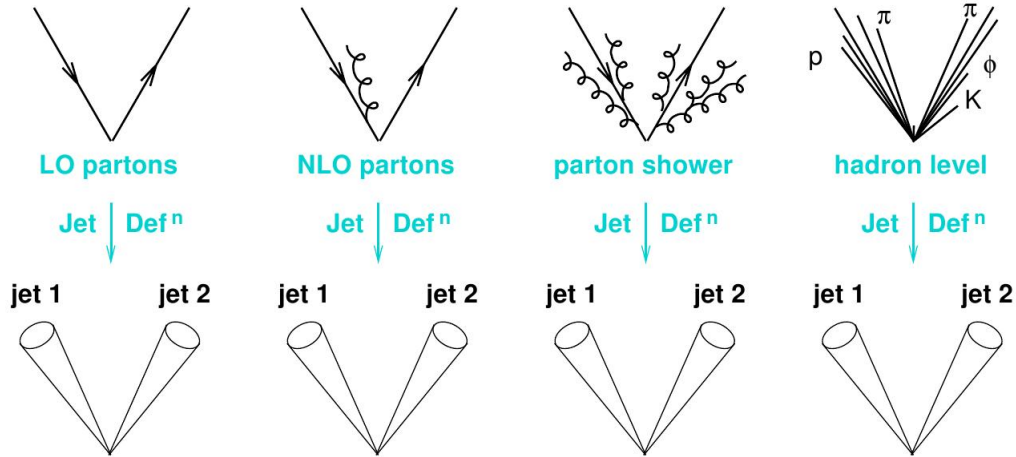


Figure 2.1: Jets reconstructed at the different levels.

**Collinear safe** - the algorithm should be insensitive to any collinear radiation in the event as well as to any splitting of particles caused by the detectors. Let's say we have a particle which deposits its energy in two neighboring calorimetric towers. Such a particle could be reconstructed as two collinear particles. If the algorithm fails in this case to generate the same jets as it would generate in the case of correctly reconstructed particle, it is collinear unsafe.

**Easy to use** - one has to be able to use the algorithm on real data.

**Detector independent** - the algorithm should be independent on the detector's properties as much as possible.

**Highly effective** - no significant jet should be missed and left unreconstructed.

**With short computing time** - demands on computer resources should be minimized. Computing time which evolves like  $\mathcal{O}(N^x)$  with  $x \leq 3$  is probably the upper boundary for practical use.

Many jet reconstruction algorithms have been developed since 1980's, but one can notice there are only two main basic approaches indeed. Cone algorithms create jets by grouping particles which lay inside a "cone" made around their tracks. On the other hand, clustering algorithms makes jets by sequential clustering particles together. I will now describe both these groups in more detail.

## 2.2 Cone algorithms

As the name suggests, cone algorithms make a virtual cone around the highest- $p_{\perp}$  particles<sup>1)</sup> (these starting particles are called **seeds**) and all particles inside the cone are proclaimed as the jet particles. A simple cone algorithm can look as follows:

- 1) Find all particles with energy above a user-specified threshold and make around them a circle of (user-specified) radius  $R = \sqrt{(\Delta\phi)^2 + (\Delta\eta)^2}$  in the  $\eta - \phi$  space, where  $\eta$  is the pseudorapidity and  $\phi$  is the azimuthal angle.
- 2) Calculate total energy and total momentum as the sum of energy and momenta of all the particles inside the circles.
- 3) Particles within the circles now form a proto-jet. Declare the non-intersecting proto-jets as final jets. If some jets do intersect, declare only the most energetic one as the final jet.

The above mentioned algorithm is very simple and fast (like  $\mathcal{O}(N)$ , where  $N$  is the number of particles), unfortunately it is not collinear safe<sup>2)</sup>. Additional improvements are therefore needed.

Also it is important that the center of the cone is aligned with the jet's momentum vector. If it is not the case, we have to set the center of the cone to the position of the momentum vector. Then we recalculate the momentum and see if it is now aligned with the center of the cone. If not, we have to repeat this step until they are aligned. This iteration process is called "stabilization".

### 2.2.1 Midpoint algorithm

Midpoint algo starts with the simple algorithm mentioned above and continues with the following steps:

- 4) Stabilize founded proto-jets.
- 5) Create new proto-jets in the midpoints between all stabilized proto-jets and also run stabilization on them.
- 6) Repeat step (5) until there are no new unique stable proto-jets found.
- 7) Split/merge intersecting proto-jets: Find the highest  $E_{\perp}$  proto-jet. If it doesn't share any particles, mark it as a final jet. Otherwise calculate fraction  $f = \frac{E_{\perp shared}}{E_{\perp highest}}$  where  $E_{\perp shared}$  is the  $E_{\perp}$  of shared particles and  $E_{\perp highest}$  is the  $E_{\perp}$  of that proto-jet. If  $f < f_{split/merge}$  (where  $f_{split/merge}$  is a user-specified parameter), then split the jets,

---

<sup>1)</sup>Depending on the level at which we are using the algorithm, as the "particles" one treats partons (parton level), hadrons (hadron level), tracks or calorimetric towers or both (detector level), depending on the particular experiment.

<sup>2)</sup>It is the  $p_{\perp}$  threshold for seeds what affects the collinear safeness.

otherwise merge them. Splitting is done by assigning all the shared particles to the nearest (in the  $\eta - \phi$  space) proto-jet, merging is done by assigning all particles (from both proto-jets) to the highest  $E_{\perp}$  proto-jet.

8) Repeat previous step until there are no proto-jets remaining.

The midpoint algorithm adopted in the DØ and CDF experiments at Tevatron was very slow,  $\mathcal{O}(N^{3.5})$ [10]! Despite of all these improvements, the midpoint algorithm is still collinear and also IR unsafe! In the light of these facts one could ask if there is an IR and collinear safe cone algorithm at all. SISCone algorithm is the answer.

## 2.2.2 SISCone algorithm

A Seedless Infrared-Safe Cone algorithm or just “SISCone” algorithm represents a state of the art cone algorithm that is not only IR-safe but also collinear-safe. I will just outline the basic steps

- 1) Put the set of current particles equal to the set of all particles in the event.
- 2) Find all stable cones of radius  $R$  for the current set of particles.
- 3) For each stable cone, create a proto-jet from the current particles contained in the cone, and add it to the list of proto-jets.
- 4) Remove all particles that are in stable cones from the list of current particles.
- 5) Repeat steps (2) - (4) until no new stable cones are found.
- 6) Run a split–merge procedure on the full list of proto-jets.

The key step in avoiding the IR and collinear unsafeness is the second one. As we know, seeds are source of the collinear unsafety. A seedless approach is therefore needed. SISCone algorithm solves this by trying to identify all distinct cones (cones having a different particle content), and testing the stability of each one. As shown on fig[], for each and every enclosure, one can always move the corresponding cone (shown as a circle in the figure) without changing its contents into a position where two particles (points) lie on its boundary. If one considers each circle whose boundary is defined by a pair of points in the set, and considers all permutations of the edge points being contained or not in the enclosure, then one will have identified all distinct circular enclosures. See article [7] how exactly is this procedure implemented in the SISCone algorithm. You can also find the proof of IR safety of the SISCone in this article.

Speed of the algorithm is  $\mathcal{O}(Nn \ln n)$ , where  $N$  is the number of particles and  $n$  is the typical number of particles in a circle of radius  $R$ .

## 2.3 Clustering algorithms

Clustering algorithms start by selecting a starting particle and then sequentially add other particles that are close enough (e.g. close in the  $\eta - \phi$  space) to the arising jet. Contrary to the cone algorithms, they have no fixed shape. This method better reflects the way the real jets are formed.

### 2.3.1 $k_{\perp}$ algorithm

- 1) For set of particles with index  $j$ , transversal momentum  $p_{\perp j}$ , position  $\phi_j, \eta_j$ , count “beam distance”  $d_j = p_{\perp j}^2$ .
- 2) For each pair of particles  $i$  and  $j$  count “distance”  $d_{ij} = \min(p_{\perp i}^2, p_{\perp j}^2) \frac{(\Delta\phi)^2 + (\Delta\eta)^2}{R^2}$ , with user-defined resolution parameter  $R$ .
- 3) Find  $d_{min} = \min(d_{ij}, d_j)$ .
- 4) If  $d_j = d_{min}$  add object  $j$  to the list of final jets, else if  $d_{ij} = d_{min}$  merge objects  $j$  and  $i$  together (sum their 4-momenta:  $p_{j'} = p_j + p_i$ ).

The algorithm is quite slow,  $\mathcal{O}(N^3)$ . Since it is collinear and IR safe, high computing demands represent its only disadvantage. However, there is a  $k_{\perp}$  implementation in FastJet software, which reaches speed of  $\mathcal{O}(N \ln N) - \mathcal{O}(N^2)$ . This makes the FastJet’s  $k_{\perp}$  algo one of the most promising jet reconstruction algorithms.

### 2.3.2 Anti- $k_{\perp}$ algorithm

There is still one small inconvenience about the  $k_{\perp}$  algorithm - it is quite sensitive to the background, since it starts the clustering from the soft particles. The anti- $k_{\perp}$  algorithm overcomes this property and starts the clustering from the hard particles. Change is in the steps (1) and (2):

- 1) ...count  $d_j = p_{\perp j}^{-2}$ .
- 2) ...count  $d_{ij} = \min(p_{\perp i}^{-2}, p_{\perp j}^{-2}) \frac{(\Delta\phi)^2 + (\Delta\eta)^2}{R^2}$

The anti- $k_{\perp}$  algorithm is also implemented in the FastJet software.

### 2.3.3 $k_{\perp}$ vs. anti- $k_{\perp}$

There is a major difference between these two algorithms in the way they response to a soft background. Suppose we reconstruct a hard event (without background) and then we add a soft background and try to run the algorithms again. The new set of jets  $J'_i$  will be different. Not only the energy of the jets will be higher by the soft energy, but also the shapes of the jets will be changed - content of particles from the hard event will not be the same in the original jets  $J_i$  compared to the new jet sets  $J'_i$ . This is called “back reaction”.

The effect of back reaction is highly suppressed for the anti- $k_{\perp}$  in comparison to the  $k_{\perp}$  algorithm [11].

The background-sensitivity of the  $k_{\perp}$  algorithm also results in another feature: the shape of the final jets reconstructed by the  $k_{\perp}$  is more or less irregular. On the other hand, jets reconstructed by the anti- $k_{\perp}$  alg. are quite round in the  $\eta - \phi$  space, likewise in the case of cone algorithms. See Figure 2.2 for  $k_{\perp}$ , anti- $k_{\perp}$  and SISCone comparison.

### 2.3.4 Resolution parameter $R$

Properties of the reconstructed jets depend also on the parameter  $R$  for the cone algorithms as well as for the clustering algorithms. Its value is usually chosen between 0.4-1.0. For higher- $p_{\perp}$  jets lower values of  $R$  are sufficient. Figure 2.3 nicely shows the  $R$ -dependence of the reconstructed jet energy. See [12] for more details.

## 2.4 FastJet

FastJet [14] is a powerful software package for jet reconstruction. It incorporates three clustering jet reconstruction algorithms: Cambridge/Aachen,  $k_{\perp}$  and anti- $k_{\perp}$ . There is also a possibility of extension for the SISCone algorithm (and others) via plugins. The source code is written in C++ and is well documented. The FastJet also features tools for background subtraction.

### 2.4.1 Speed

As mentioned above, the (anti-) $k_{\perp}$  algorithm embodies computational speed of  $\mathcal{O}(N^3)$ , which makes it very impractical for “everyday use”. Assorting the pairs  $i, j$  and calculating the distance  $d_{i,j}$  is an  $\mathcal{O}(N^2)$  demanding step. Choosing the minimum  $d_{i,j}, d_j$  is an  $\mathcal{O}(N^2)$  operation done  $N$ -times. This step dominates, resulting in the total complexity of  $\mathcal{O}(N^3)$ . FastJet overcomes this inconvenience by looking for the “nearest” (with minimal  $d_{ij}$ ) particles only among the geometrically nearest (with minimal  $r_{ij} \equiv \sqrt{(\Delta\phi)^2 + (\Delta\eta)^2}$ ) neighbors  $G_i$ :

1. For each particle  $i$  establish its (geometrically) nearest neighbor  $G_i$  and construct the arrays of the  $d_{iG_i}$  and  $d_{iB}$ . // $\mathcal{O}(N) \times N$
2. Find the minimal value  $d_{min}$  of the  $d_{iG_i}, d_{iB}$ . // $\mathcal{O}(N) \times N$
3. Merge or remove the particles corresponding to  $d_{min}$  as appropriate. //done  $N$ -times
4. Identify which particles’ nearest neighbors have changed and update the arrays of  $d_{iG_i}$  and  $d_{iB}$ . If any particles are left go to step 2. // $\mathcal{O}(N) \times N$

It is apparent that the total complexity of the algorithm is now  $\mathcal{O}(N^2)$ . Steps 1,2 and 4 can be yet more speeded up to  $\mathcal{O}(N \ln N)$  [15] by using a special structure known from

computer science - the Voroni diagrams. By constructing these diagrams, it is possible to find the nearest neighbor with  $\mathcal{O}(N \ln N)$  operations. Also steps 2 and 4 can be then performed only with  $\mathcal{O}(N \ln N)$  operations.

FastJet implements both  $N^2$  and  $N \ln N$  variants of the  $k_{\perp}$  algorithm. Moreover, fast variants of the anti- $k_T$  and Cambridge/Aachen algorithms are implemented in the same manner. [Figure 2.4](#) shows comparison of speed of various jet finders.

## 2.4.2 Jet areas

In heavy ion collisions it is necessary to subtract the underlying event background. This can be done e.g. by putting cuts on  $p_{\perp}$ . This solution is however not very satisfying, since low cuts leave too much of background and high cuts can introduce potential biases in the investigation of jet-quenching effects. FastJet includes tools for background subtraction after running the reconstruction algorithm. It uses concept of **jet areas** for this purpose. FastJet proposes three definitions of the jet area:

- Active area - Many soft “ghost” particles are added to the event and the reconstructing procedure is done once more. Soft ghosts don’t affect the content of original hard particles in reconstructed jets, since the FastJet algorithms are IR safe. The jet area is then proportional to the number of ghost contained in the jet. Next to the original hard jets there are also many soft “ghost” jets found.
- Passive area - One soft ghost is added to the event. One looks for the jet which contains the ghost. This is repeated many times and the jet area is proportional to the probability of finding the ghost in the jet.
- Voronoi area - Voronoi diagrams are constructed for the event and the jet area is calculated as the sum of voronoi areas of jet’s constituent particles.

After calculating the jet areas  $A_j$  one calculates noise distribution in the event  $\rho = \text{med}(\frac{p_{\perp}^j}{A_j})$  (by using the median the hard jets are excluded and only the soft “ghost” jets are used for the noise distribution calculation). Jet’s  $p_{\perp}$  is then corrected:

$$p_{\perp}^{corr} = p_{\perp} - A\rho \tag{2.1}$$

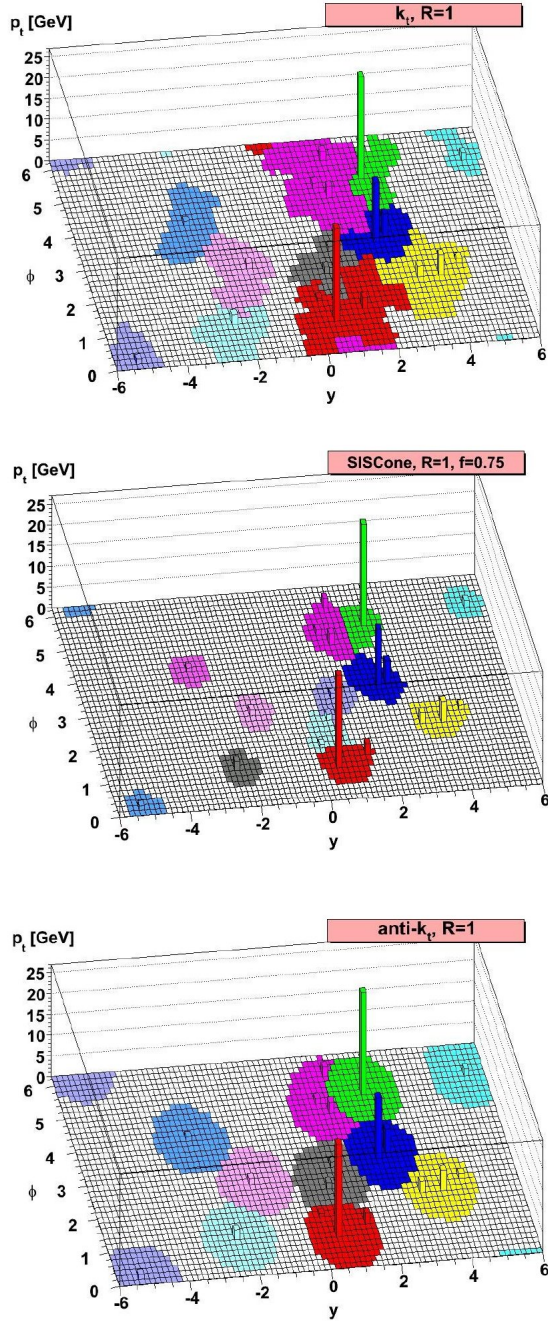


Figure 2.2: Jet shapes reconstructed by  $k_{\perp}$ ,  $anti-k_{\perp}$  and SISCone algorithms in a sample parton-level hard event generated with Herwig supplemented with many random soft particles (“ghosts”).

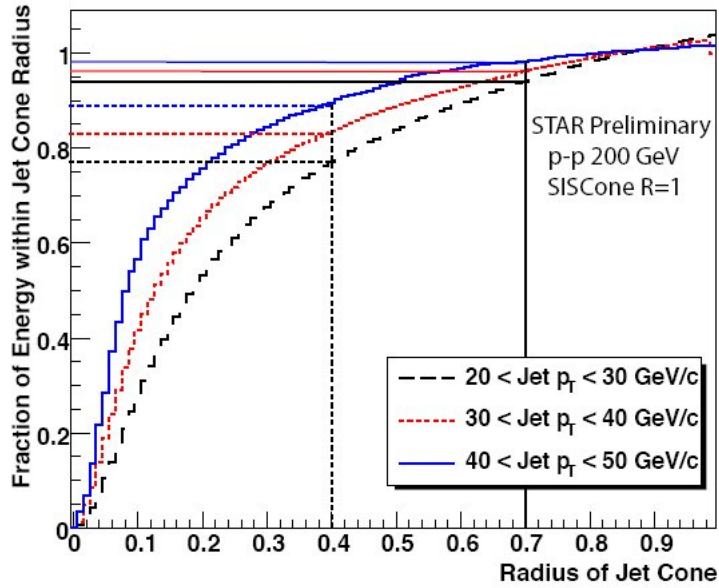


Figure 2.3: The fraction of energy within a jet cone of radius  $R$ . As the total energy is meant the energy of the jet with  $R=1$ .

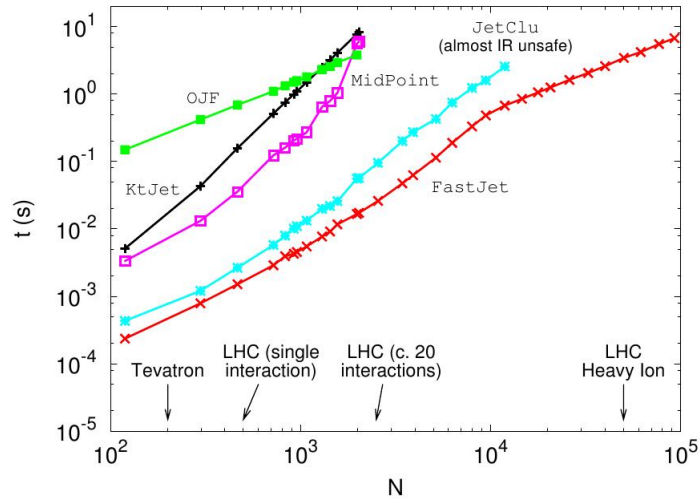


Figure 2.4: CPU time vs. initial number of particles of several widely used jet finding algorithms and FastJet  $N^2 k_{\perp}$  variant.

# Chapter 3

## STAR Experiment

### 3.1 RHIC

Relativistic Heavy Ion Collider (RHIC) is the biggest<sup>1)</sup> operating heavy-ion collider in the world. It came to operation in 2000. Since that year it is still under way without any serious problems. It is situated at the Brookhaven National Laboratory on the Long Island, NY.

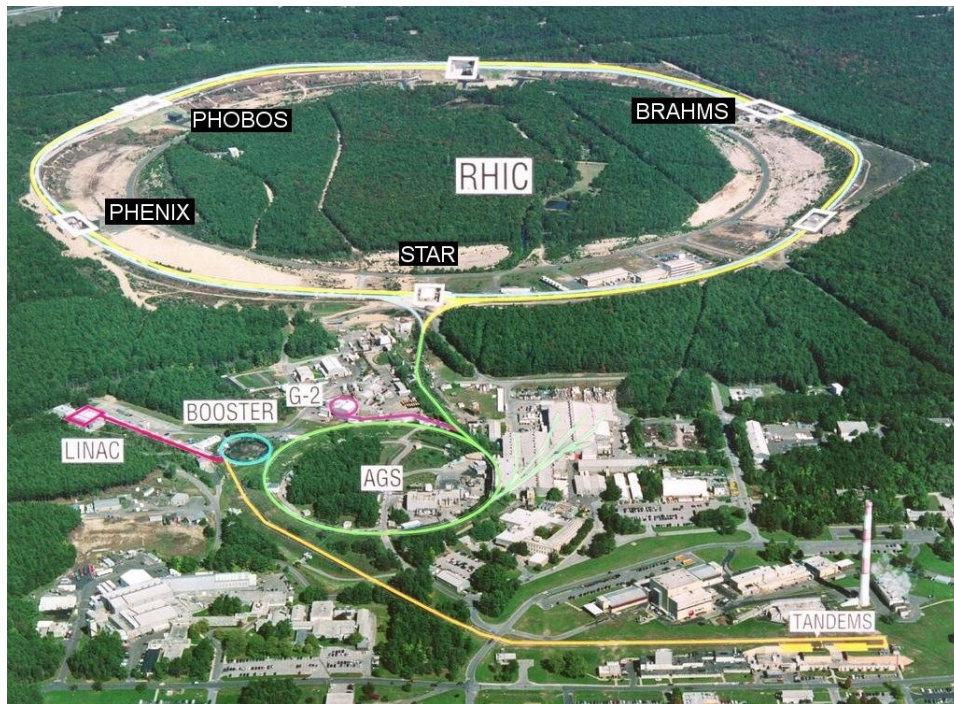


Figure 3.1: Aerial photo of the RHIC and a part of the BNL complex. Positions of all 4 RHIC experiments are also marked.

<sup>1)</sup>In the terms of energy: typical center-of-mass energy per nucleon-nucleon pair in Au+Au collisions is  $\sqrt{s} = 200$  GeV.

RHIC is composed of two separated rings which are 3834 m long in circumference with six intersecting sections - interaction points. Therefore it is not necessary to collide particles with the same mass and with the opposite charge, but almost any combination of our choice. The most frequent combinations of collided particles are Au+Au and for arbitrary measurements p+p, d+Au, Cu+Cu. Together with the heavy ion program, there is also a very important program of colliding polarized protons at RHIC.

Before the particles enter the RHIC ring, they are pre accelerated by a whole system of pre-accelerators: as first the Tandem Van de Graaff (for ions)/the Linac (for protons), then the Booster and finally the Alternating Gradient Synchrotron (AGS).

There have been four detector systems operating at RHIC:

- STAR (6 o'clock position at the RHIC)
- PHENIX (8 o'clock)
- PHOBOS (10 o'clock)
- BRAHMS (2 o'clock)

PHOBOS and BRAHMS were specialized experiments and finished their operation in 2005 and 2006 respectively. Both STAR and PHENIX are still active. STAR features a Time Projection Chamber (TPC) detector with full azimuthal coverage, which is ideal for charged tracks reconstruction. On the other hand PHENIX is designed with detectors covering only a part of full-azimuth, since it is equipped with very precise and hence very expensive electromagnetic calorimeters.

## 3.2 STAR

STAR is an acronym for the Solenoidal Tracker at RHIC. This large detector is designed to observe most of the particles (charged and also neutral) produced in nuclear collisions at RHIC. Its primary goals are to search for signatures of quark-gluon plasma, investigate the behavior of strongly interacting matter at high energy density, and measure gluon polarization using highly polarized protons.

Most of its subdetectors have full azimuthal and mid-rapidity coverage. The whole detector system is covered by a large solenoidal magnet which creates an uniform magnetic field of 0.5 Tesla. This field bends trajectories of charged particles and makes it possible to determine their momenta. These tracks are reconstructed in the main sub-detector - the Time Projection Chamber (TPC). When going through the TPC, also the energy lost  $dE/dx$  of the particle is measured. Then it is possible to identify the particle. When one knows both momentum and mass of a particle, it is possible to calculate its energy. However, this holds only for charged particles. Neutral particles will go through the TPC without leaving any evidence of their presence. Photons and particles which decay to photons (like  $\pi^0$ ) will deposit their energy in the outermost laying detector - the electromagnetic calorimeter, but some neutral particles like neutrons can leave also

the electromagnetic calorimeter deponing almost no energy in there and therefore remain undetected.

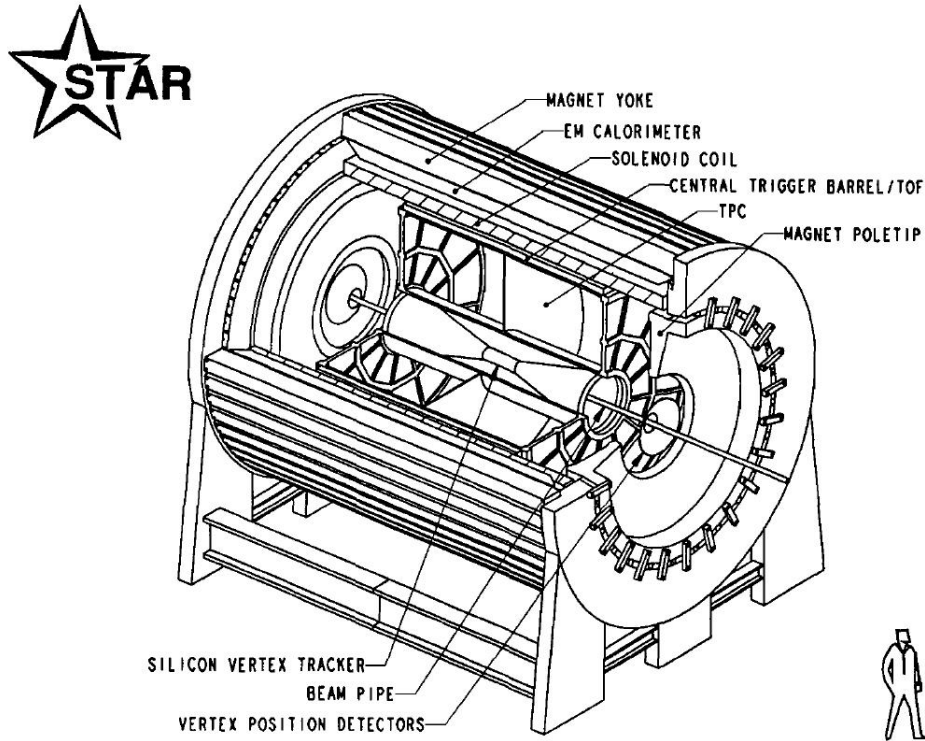


Figure 3.2: Sketch of the STAR detector.

Now we will take a look at two subdetectors that are crucial for my analysis.

### 3.2.1 Time Projection Chamber

The Time Projection Chamber [19] is the heart of STAR. It is a 4.2 meter long barrel with outer radius of 2.0m filled with gaseous argon (90%) and methane (10%) at the atmospheric pressure. The cylinder is divided into two sections by a thin high-voltage carbon coated annulus membrane. This membrane forms an uniform electric field in the longitudinal direction. A charged particle which goes through the TPC ionizes the gas around its track. Ionization electrons start to drift along the electric field direction towards the end-cap. The end-caps contain  $2 \times 70,000$  pads with anode multi-wire proportional chambers (MPWC) in which the electron signal is amplified and recorded. MPWC's wires form a grid, therefore it is possible to determine two coordinates  $(x,y)$  of each track segment, the  $z$  (longitudinal) coordinate is determined from the drift time. All together we obtain the necessary information for a 3-dimensional track reconstruction of each charged particle coming through the TPC. STAR TPC also provides  $dE/dx$  measurements. Its acceptance

for tracking and  $dE/dx$  measurement is  $|\eta| < 1.0$  at full efficiency, and extends up to  $|\eta| < 1.8$  with reduced efficiency and resolution. The spacial resolution is  $460 \mu\text{m}$  in  $x, y$  and  $700 \mu\text{m}$  in  $z$ . A disadvantage of the TPC is its relative slowness - the drift time from the membrane to the end-cap is  $\sim 40 \mu\text{s}$ .

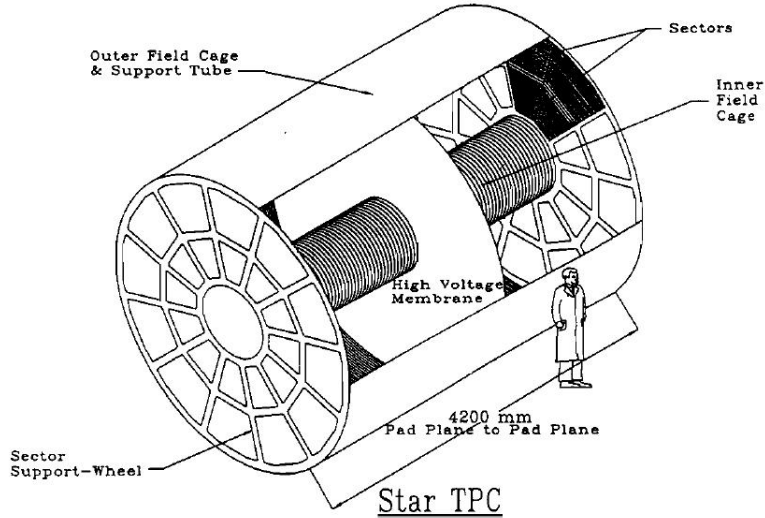


Figure 3.3: View of the STAR Time Projection Chamber.

### 3.2.2 Electromagnetic Calorimeter

The STAR Barrel Electromagnetic Calorimeter (EMC) [18] is made of 41 layers of lead and scintillator. It has full azimuthal coverage and pseudorapidity coverage  $0 < |\eta| < 1$ . It is divided into 120 segments in azimuthal angle and 40 segments in pseudorapidity. Therefore there are 4800 calorimetric towers, each of them with individual read out. Resolution (effective size of the towers) of the EMC is  $0.05 \times 0.05$  ( $\Delta\phi \times \Delta\eta$ ). Its main goal is to measure and trigger on the transverse energy deposition in the collisions, mainly from  $e^+, e^-$  and photons.

### 3.2.3 Upgrades

After almost one decade, the STAR detector is still not going to be retired. Many new detectors have been installed in recent time and there are still plans for future upgrades.

#### Forward Meson Spectrometer

The Forward Meson Spectrometer (FMS) is a Pb-glass calorimeter, covering  $2.5 < \eta < 4.0$ . Its task is to measure the energy of low- $p_{\perp}$  mesons. It has been operational since run 8.

## **Time of Flight**

The Time of Flight (TOF) is a detector which is used for particle identification. It measures the time it takes to a particle to fly through the TOF. Then it is possible to calculate its speed. In combination with knowledge of the particle's momentum, it is possible to identify the particle. It has been operational since run 9.

## **Heavy Flavor Tracker**

Heavy Flavor Tracker (HFT) is designed to precisely determine the secondary vertex of rapidly decaying particles containing heavy quarks, like  $D^0$  or  $B^0$ . It consists of several layers of pixel detectors. It should also, together with the Silicon Strip Detectors, improve the TPC's tracking abilities.

# Chapter 4

## Measurement of Jet $j_{\perp}$

### 4.1 Jet $j_{\perp}$

The variable  $j_{\perp}$  is defined as the projection of particle's momentum to the plane perpendicular to the jet axis. See [Figure 4.1](#) for better imagination.

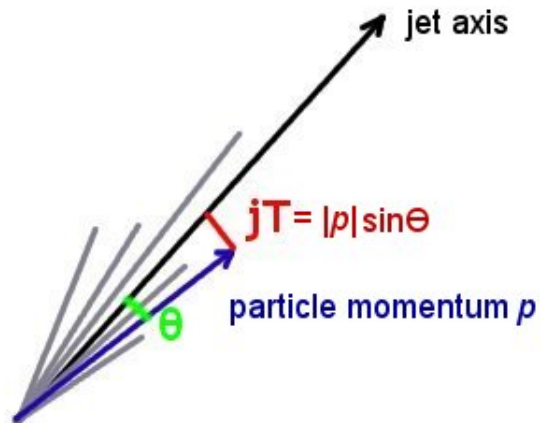


Figure 4.1: Sketch of the  $j_{\perp}$ .

What does the  $j_{\perp}$  distribution tells us about a jet? It gives us a basic information about the jet shape. Higher  $j_{\perp}$  values mean that the jet is more spread, containing also particles with lower  $p_{\perp}$ . Low  $j_{\perp}$  values represent particles which form a narrow cone. These information can be valuable when one studies e.g. the quark gluon plasma.

## 4.2 Analysis

### Data

The data used for the analysis are min-bias<sup>1</sup> data from d+Au collisions from the run 08. Charged tracks from the TPC and neutral (coming from the neutral particles) energy deposits in the BEMC were used for the jet reconstruction. The analysis was performed on a sample of 10.000.000 events. The jets were reconstructed using the FastJet software. The anti- $k_{\perp}$  algorithm was mainly used for this purpose. There was a pseudorapidity cut applied:  $|\eta| < 0.9 - R$  ( $R$  is the resolution parameter used for the jet reconstruction). Jets with axis pointing out of this interval were not accepted. Also a  $p_{\perp}$  cut was put on - only those jets with  $p_{\perp} > 5$  GeV were studied.

All the data are still uncorrected for the detector effects.

### Results

**Jet  $p_{\perp}$  spectra:** In this paragraph I will present the  $p_{\perp}$  spectra of the reconstructed jets. The jet  $p_{\perp}$  was corrected for the background effect by techniques described in the section 2.4.2, concretely the active areas reconstructed by the  $k_{\perp}$  algorithm<sup>2)</sup> were used. However, the background is unisotropic in the d+Au collisions and poses a  $\eta$  dependence. Nevertheless one can show [9] that this dependence can be approximated by a simple linear function in the pseudorapidity region of  $|\eta| < 0.4$ , which is the fiducial acceptance for jets with  $R = 0.5$  (see Figure 4.2).

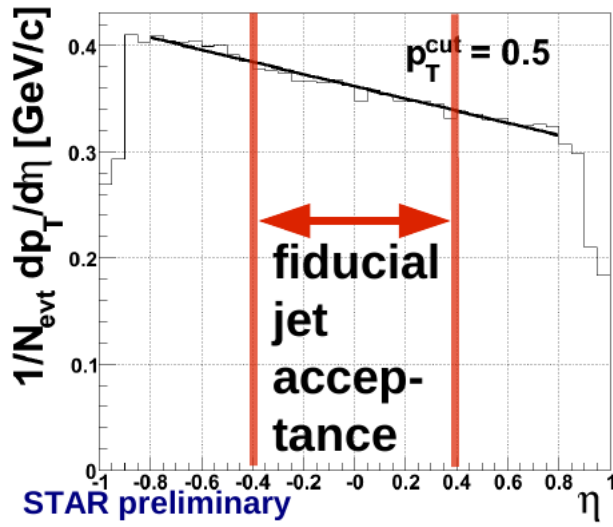


Figure 4.2: The  $\eta$ -dependence of the background in the d+Au collisions [9].

<sup>1</sup>No  $p_{\perp}$  trigger was used.

<sup>2</sup>Jet areas reconstructed by the  $k_{\perp}$  algorithm are larger than if they are reconstructed by the anti- $k_{\perp}$  algorithm. Therefore they are more suitable for the background subtraction.

All together, the corrected transversal momentum is then

$$p_{\perp}^{corr} = p_{\perp} - A\rho(1 + c\eta), \quad (4.1)$$

where  $p_{\perp}$  is the uncorrected transversal momentum,  $A$  is the jet area determined by the  $k_{\perp}$  algorithm,  $\rho$  is the background energy density<sup>3)</sup> calculated as mentioned in the section 2.4.2,  $c$  is a constant determined from experimental fits [9] (its value is  $\sim -1.5$ ).

The  $p_{\perp}$  spectra are drawn for different values of the  $p_{\perp}$  cut applied on the jet particles at Figure 4.3.

The second set of the  $p_{\perp}$  spectra histograms shown at Figure 4.4 differs in the resolution parameter  $R$ . It can be seen that the resolution parameter doesn't affect the distribution as the value of the  $p_{\perp}$  cut.

At the Figure 4.5 the  $p_{\perp}$  spectra obtained by the  $k_{\perp}$  and anti- $k_{\perp}$  algorithm are compared. One can see that after the background subtraction the spectra reconstructed by the  $k_{\perp}$  and anti- $k_{\perp}$  algorithm are similar.

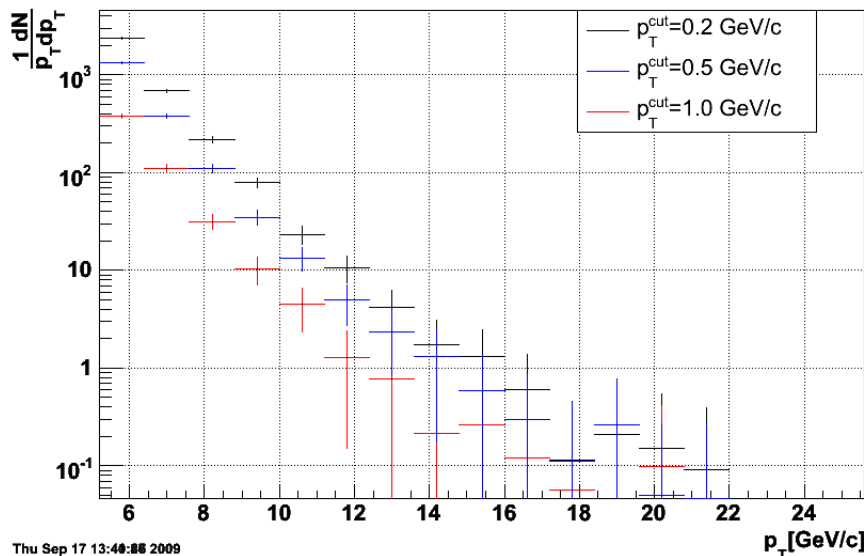


Figure 4.3: The  $p_{\perp}$  spectra of reconstructed jets for various background  $p_{\perp}$  cuts. Jets were reconstructed by the anti- $k_{\perp}$  algorithm,  $R = 0.5$ .

Figure 4.6 compares calculated jet areas as a function of  $p_{\perp}$  for the  $k_{\perp}$  and anti- $k_{\perp}$  algorithms. It is clear that the  $k_{\perp}$  algorithm tends to form jets with larger areas than the anti- $k_{\perp}$  algorithm at the same  $p_{\perp}$ .

<sup>3)</sup>Background energy density in the d+Au collisions is e.g. for the  $p_{\perp}^{cut} = 0.5$  GeV/c approximately 1GeV/unit area

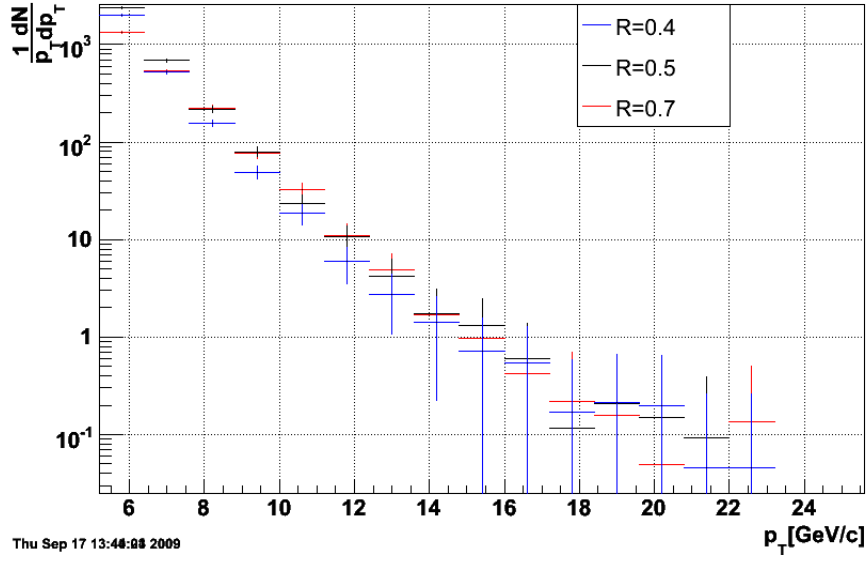


Figure 4.4: The  $p_{\perp}$  spectra of reconstructed jets for various values of the resolution parameter  $R$ . Jets were reconstructed by the anti- $k_{\perp}$  algorithm,  $p_{\perp}^{cut} = 0.2$  GeV.

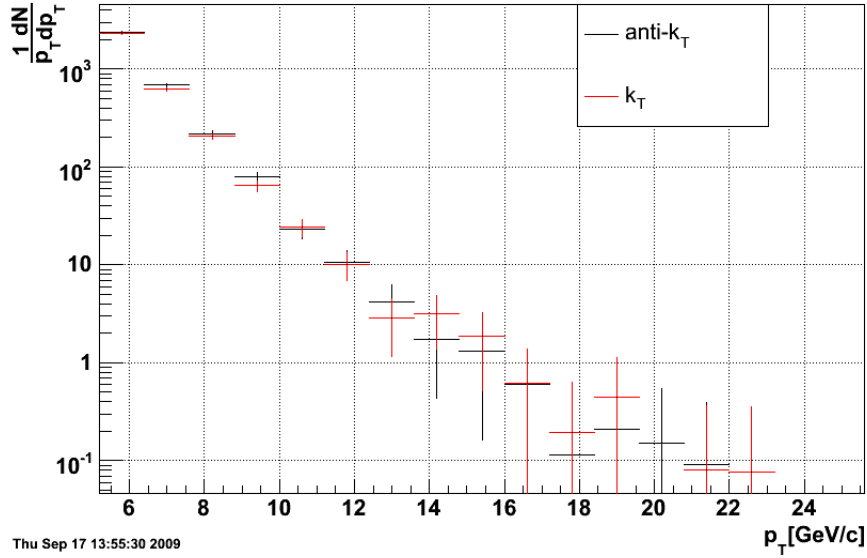


Figure 4.5: The  $p_{\perp}$  spectra of jets for two variants of the jet reconstruction algorithm -  $k_{\perp}$  and anti- $k_{\perp}$ .  $R = 0.5$ ,  $p_{\perp}^{cut} = 0.2$  GeV.

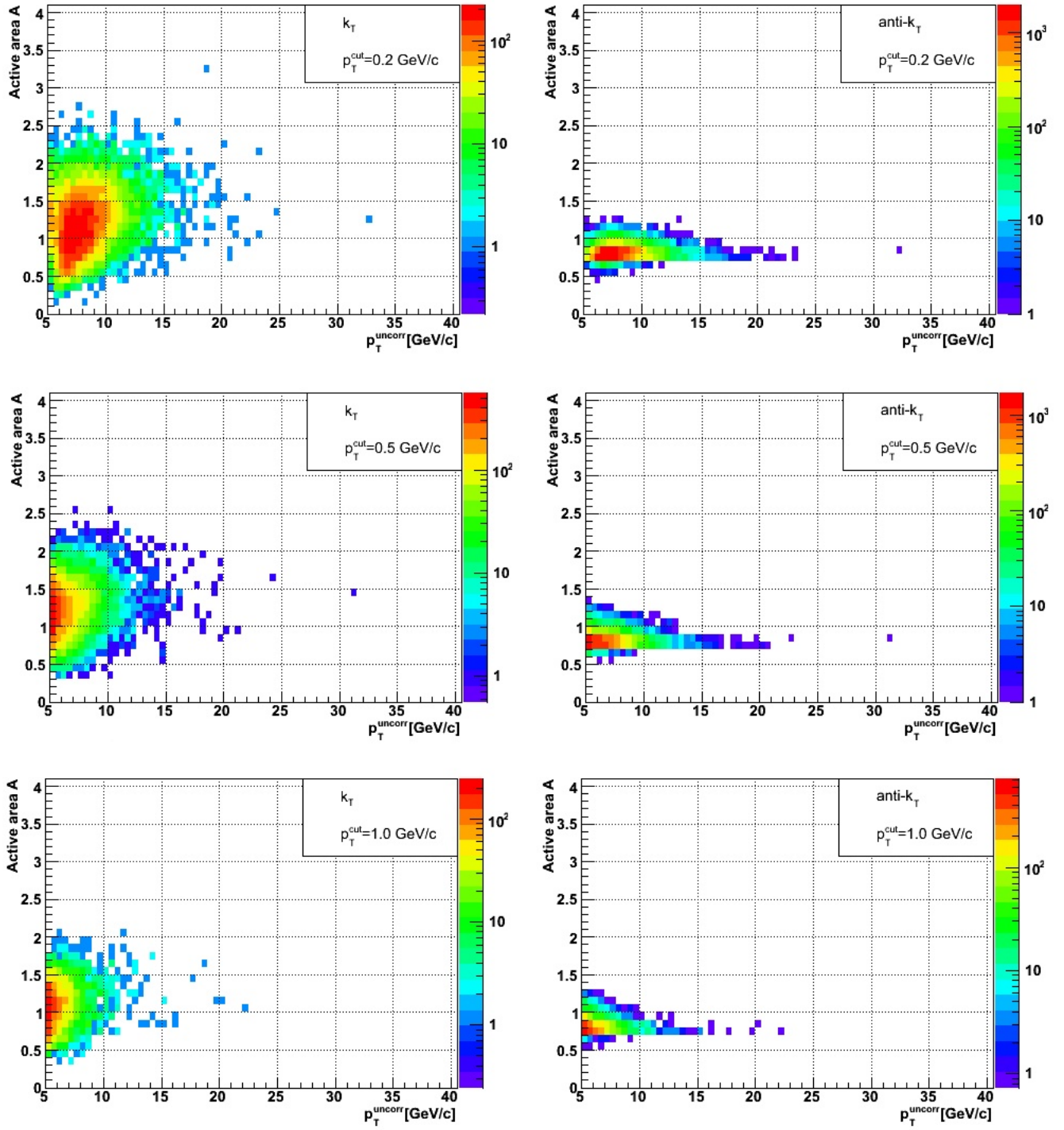


Figure 4.6: Jet (active) areas as a function of (uncorrected)  $p_{\perp}$ .

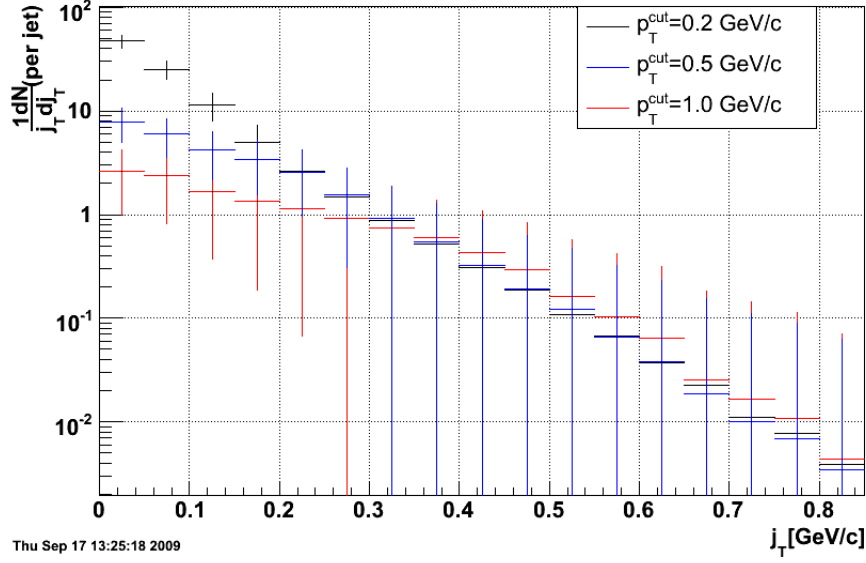


Figure 4.7: Distribution of  $j_{\perp}$  for various background  $p_{\perp}$  cuts. Jets were reconstructed by the anti- $k_{\perp}$  algorithm,  $R = 0.5$ .

**$j_{\perp}$  distributions:** I will present the main results - the  $j_{\perp}$  distributions - in this paragraph. Although these data are not corrected for the background and detector effects,  $j_{\perp}$  is quite robust variable, depending mainly on the precision of finding the jet axis. Therefore it is anticipated that the influence of these corrections will not be significant.

Figure 4.7 shows  $j_{\perp}$  distributions for three distinct background  $p_{\perp}$  cuts -  $p_{\perp}^{cut} = 0.2, 0.5, 1.0$  GeV/c. This means only the particles with  $p_{\perp} > p_{\perp}^{cut}$  were added to the jet. It is clear that low- $j_{\perp}$ s are suppressed for the higher  $p_{\perp}$  cuts. The suppression of low  $j_{\perp}$  for higher  $p_{\perp}$  cuts is not well understood yet and it will be a subject of further study.

Different  $j_{\perp}$  distributions for three values of the resolution parameter ( $R = 0.7, 0.5, 0.4$ ) are shown at the Figure 4.8. Jets with large  $R$  may contain particles with high  $j_{\perp}$  (since the jets with large  $R$  may contain particles with trajectories forming a large angle with the jet axis), therefore the  $j_{\perp}$  distribution is not so steep in their case. However the observed difference is within statistical errors.

Next figure (Figure 4.9) shows the  $j_{\perp}$  distributions for the anti- $k_{\perp}$  and  $k_{\perp}$  algorithms. No statistically significant difference between the studied jet reconstruction algorithms is observed.

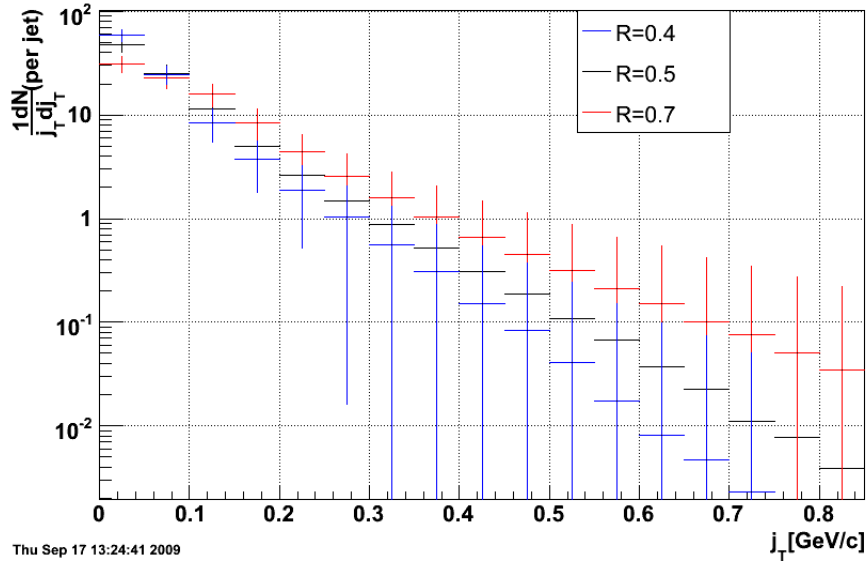


Figure 4.8: Distribution of  $j_{\perp}$  for various values of the resolution parameter  $R$ . Jets were reconstructed by the anti- $k_{\perp}$  algorithm,  $p_{\perp}^{cut} = 0.2$  GeV.

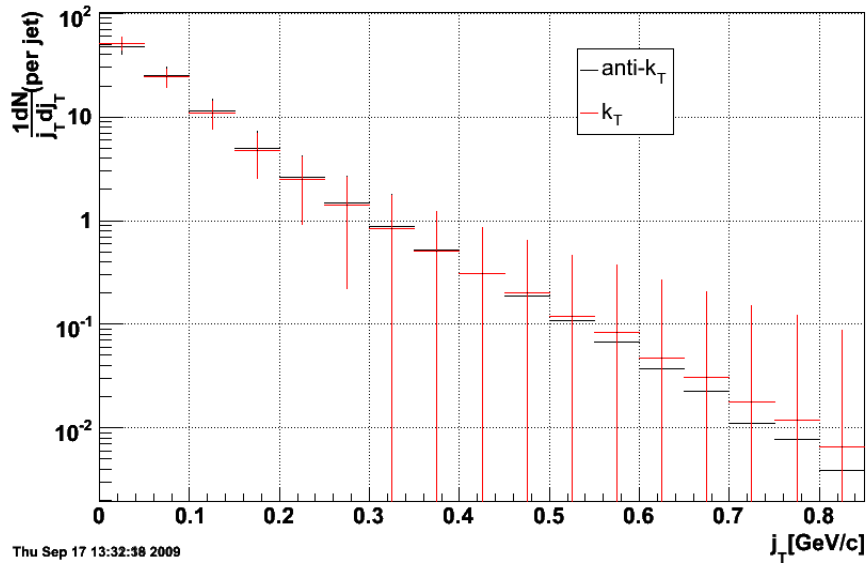


Figure 4.9: Two  $j_{\perp}$  distributions for different jet reconstruction algorithms.  $R = 0.5$ ,  $p_{\perp}^{cut} = 0.2$  GeV/c.

## Summary and Outlook

The main subject of this work was a review of various modern jet reconstruction algorithms and their practical application to jet reconstruction in d+Au collisions at  $\sqrt{s_{NN}} = 200$  GeV measured by the STAR collaboration at RHIC.

In particular, I made first analyses using the  $k_{\perp}$  and anti- $k_{\perp}$  jet reconstruction algorithms and extracted raw  $p_{\perp}$  spectra and  $j_{\perp}$  distributions of jets in minimally biased d+Au data sample. Both the jet  $p_{\perp}$  spectra and  $j_{\perp}$  distributions were studied in detail for different resolution parameters  $R$  and several distinct  $p_T$  cuts on background. The measured distributions are not yet corrected for various detector effects (limited acceptance, dead tower in the electromagnetic calorimeter etc.). These corrections are beyond the scope of this work and will be performed within my MSc thesis.

In addition, the analysis of several triggered data samples ("high-tower" data sets) will also be performed and will enable to extend the reach of reconstructed transverse momenta of jets.

Ultimately, the fully corrected  $p_{\perp}$  and  $j_{\perp}$  distributions will be compared to those from p+p and Au+Au collisions to estimate size of cold nuclear matter effects and infer more details on properties of hot and dense nuclear matter created at RHIC.

# Bibliography

- [1] STAR Collaboration - J. Adams *et al.*, Nucl. Phys. A 757, 102 (2005).
- [2] PHENIX Collaboration - K. Adcox *et al.*, Nucl. Phys. A 757, 184 (2005).
- [3] E. Bruna, Eur. Phys. J. C 62, 133-137 (2009); J. Putschke, Eur. Phys. J. C 62, 629-635 (2009); S. Salur, Eur. Phys. J. C 61, 761-767 (2009).
- [4] T. W. Henry, “Reconstruction And Attributes Of Jets Observed In  $\sqrt{s} = 200$  GeV Proton-Proton and Deuteron-Gold Collisions At STAR”, Texas A&M University, 2006.
- [5] G. C. Blazey *et al.*, [arXiv:hep-ex/0005012v2](https://arxiv.org/abs/hep-ex/0005012v2).
- [6] D. Enterria, [arXiv:0902.2011v2](https://arxiv.org/abs/0902.2011v2).
- [7] G. P. Salam, G. Soyez, JHEP0705:086, 2007, [arXiv:0704.0292v2](https://arxiv.org/abs/0704.0292v2).
- [8] M. E. Peskin, D. V. Schroeder, “An Introduction To Quantum Field Theory” (Westview, 1995).
- [9] J. Kapitán (STAR), poster at the Quark Matter 2009 conference, <http://qm09.phys.utk.edu/indico/getFile.py/access?contribId=743&sessionId=44&resId=0&materialId=poster&confId=1>.
- [10] J. Miner, “Comparison of Jet reconstruction Algorithms”, 2006.
- [11] M. Cacciari, G. P. Salam, G. Soyez, JHEP0804:063, 2008, [arXiv:0802.1189v2](https://arxiv.org/abs/0802.1189v2).
- [12] H. Caines, [arXiv:0907.3460v1](https://arxiv.org/abs/0907.3460v1).
- [13] STAR Collaboration - J. Adams *et al.*, Phys. Rev. Lett. 91, 072304 (2003); Phys. Rev. Lett. 97, 162301 (2006).
- [14] FastJet webpage, <http://www.lpthe.jussieu.fr/~salam/fastjet/>.
- [15] M. Cacciari, G. P. Salam, Phys. Lett. B 641, 57-61 (2006), [arXiv:hep-ph/0512210v2](https://arxiv.org/abs/hep-ph/0512210v2).
- [16] Wikipedia webpage of the RHIC, [http://en.wikipedia.org/wiki/Relativistic\\_Heavy\\_Ion\\_Collider](http://en.wikipedia.org/wiki/Relativistic_Heavy_Ion_Collider).
- [17] STAR Collaboration, “STAR Conceptual Design Report”, 1992.

[18] M. Beddo *et al.*, Nucl. Instrum. Meth. A 499, 725 (2003).

[19] M. Anderson *et al.*, Nucl. Instrum. Meth. A 499, 659 (2003).

## Acknowledgements

I would like to thank to Jana Bielčíková for her guidance and help with this work and for her infinite patience. I would also like to thank to Jan Kapitán for his precious advices and suggestions.